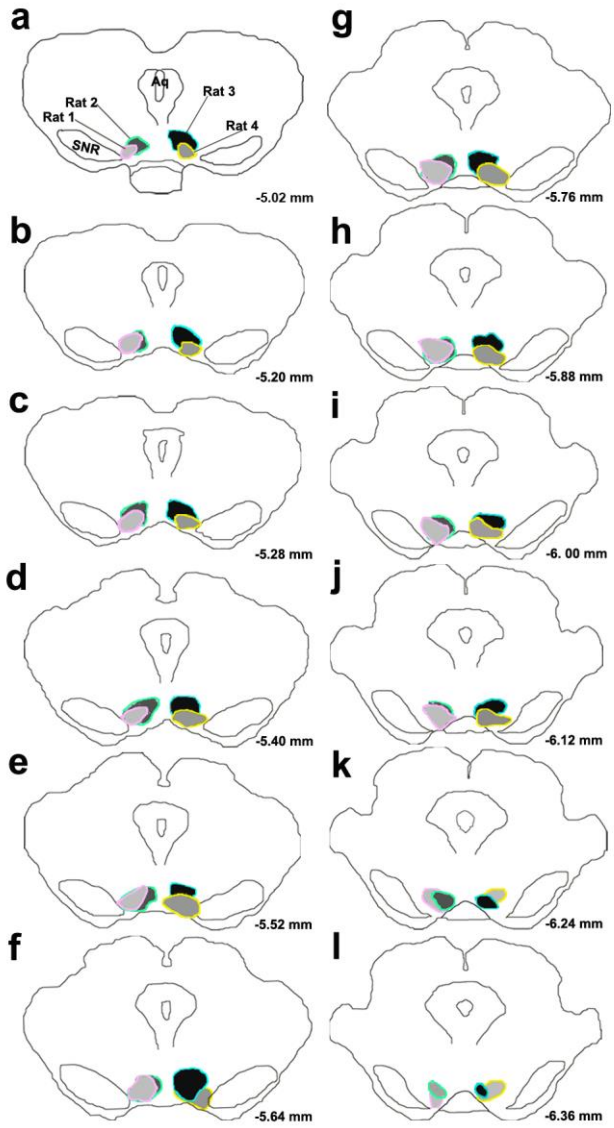

Supplementary Figure 1 Schematic representation of FG injected sites within the rat VTA (4 rats). (a-l) Diagrams corresponding to the injection sites arranged rostrocaudally from -5.02 mm to -6.36 mm. Aq, aqueduct; SNR, substantia nigra reticulata.

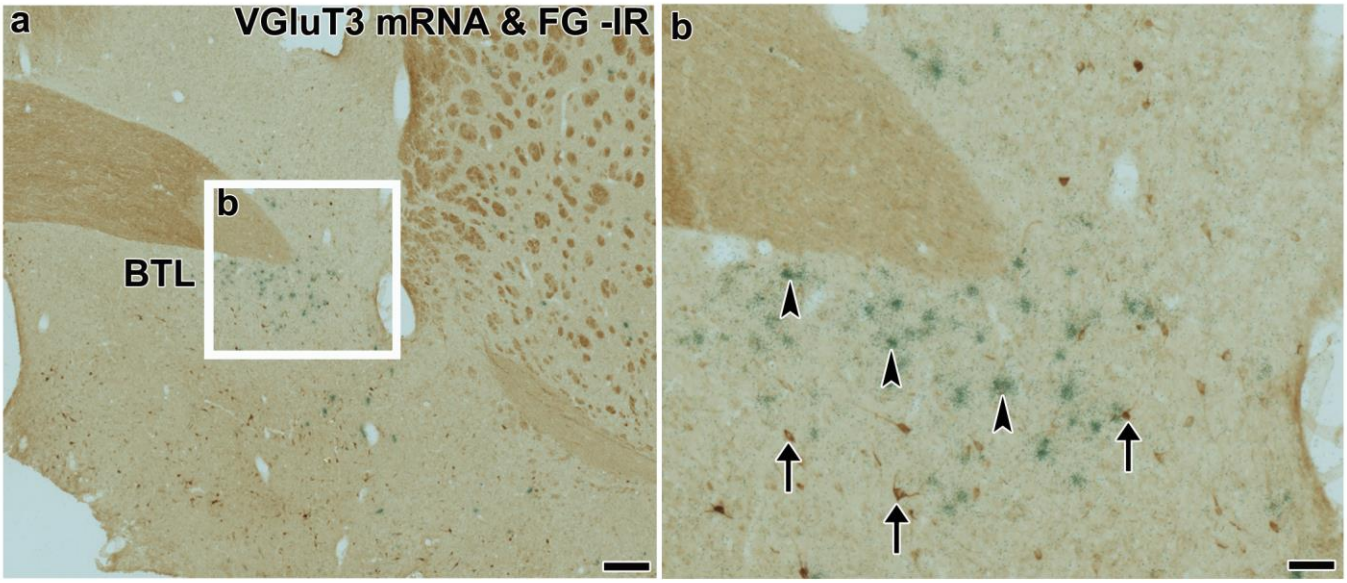

Supplementary Figure 2 Neurons from the bed nucleus of the stria terminalis that project to the VTA lack VGluT3 mRNA.

(a) Low magnification of FG-immunoreactive (FG-IR) neurons within the lateral division of the bed nucleus of the stria terminalis (BTL). (b) At high magnification these FG-IR neurons are shown to lack VGluT3 mRNA (green aggregated grains). FG-IR cells (arrows) are intermixed with neurons that express VGluT3 mRNA (arrowheads). Bars: (a) 175 µm; (b) 50 µm.

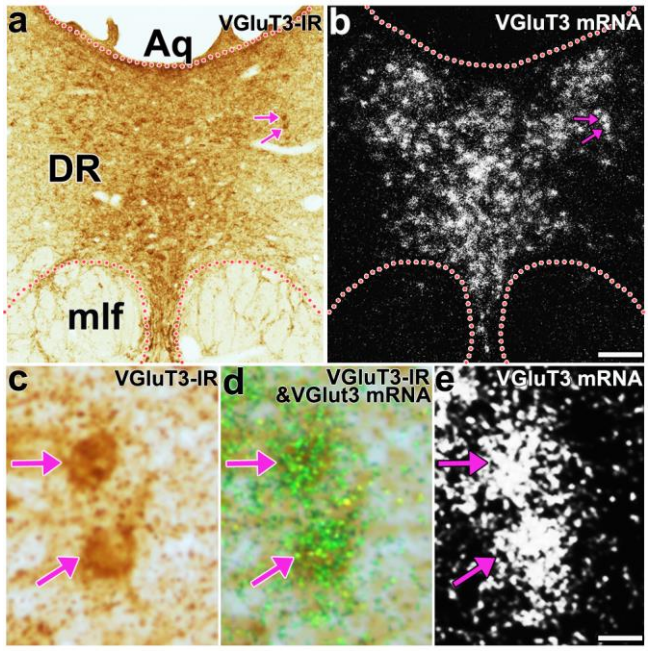

Supplementary Figure 3 Detection of VGluT3 immunoreactivity in DR neurons expressing VGluT3 mRNA.

(a-b) DR neurons that contain VGluT3-immunoreactivity (VGluT3-IR, brown under bright field microscopy) co-express VGluT3 mRNA (white grain aggregates under epiluminescence microscopy). (c-e) High magnification of two neurons co-expressing VGluT3-IR and VGluT3 mRNA which are indicated by arrows in a-b. Aq, aqueduct; mlf, medial longitudinal fasciculs; DR, dorsal raphe. Bars: (b) 238 μm; (e) 50 μm.

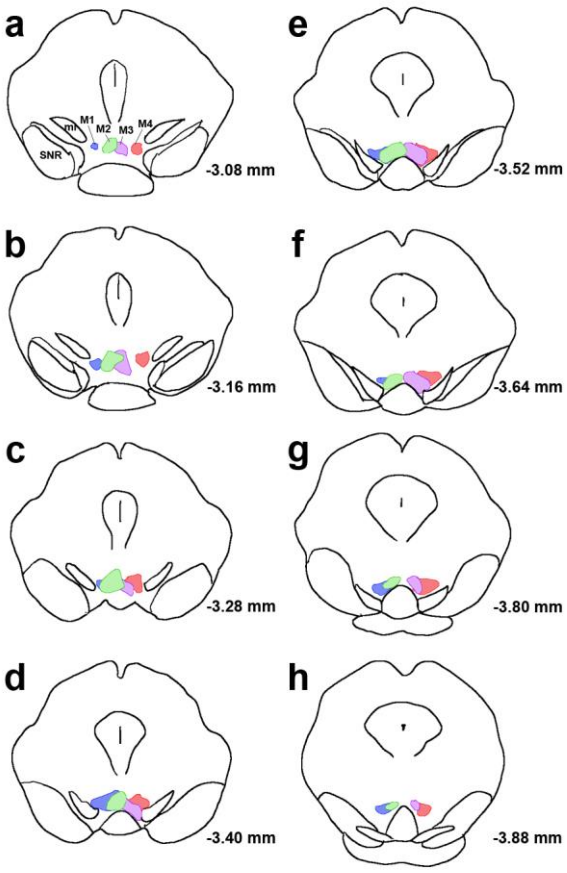

Supplementary Figure 4 Schematic representation of FG injected sites within the mouse VTA (4 mice).

(a-h) Diagrams corresponding to the injection sites arranged rostrocaudally from -3.08 mm to -3.88 mm. ml, medial lemniscus; SNR, substantia nigra reticulata.

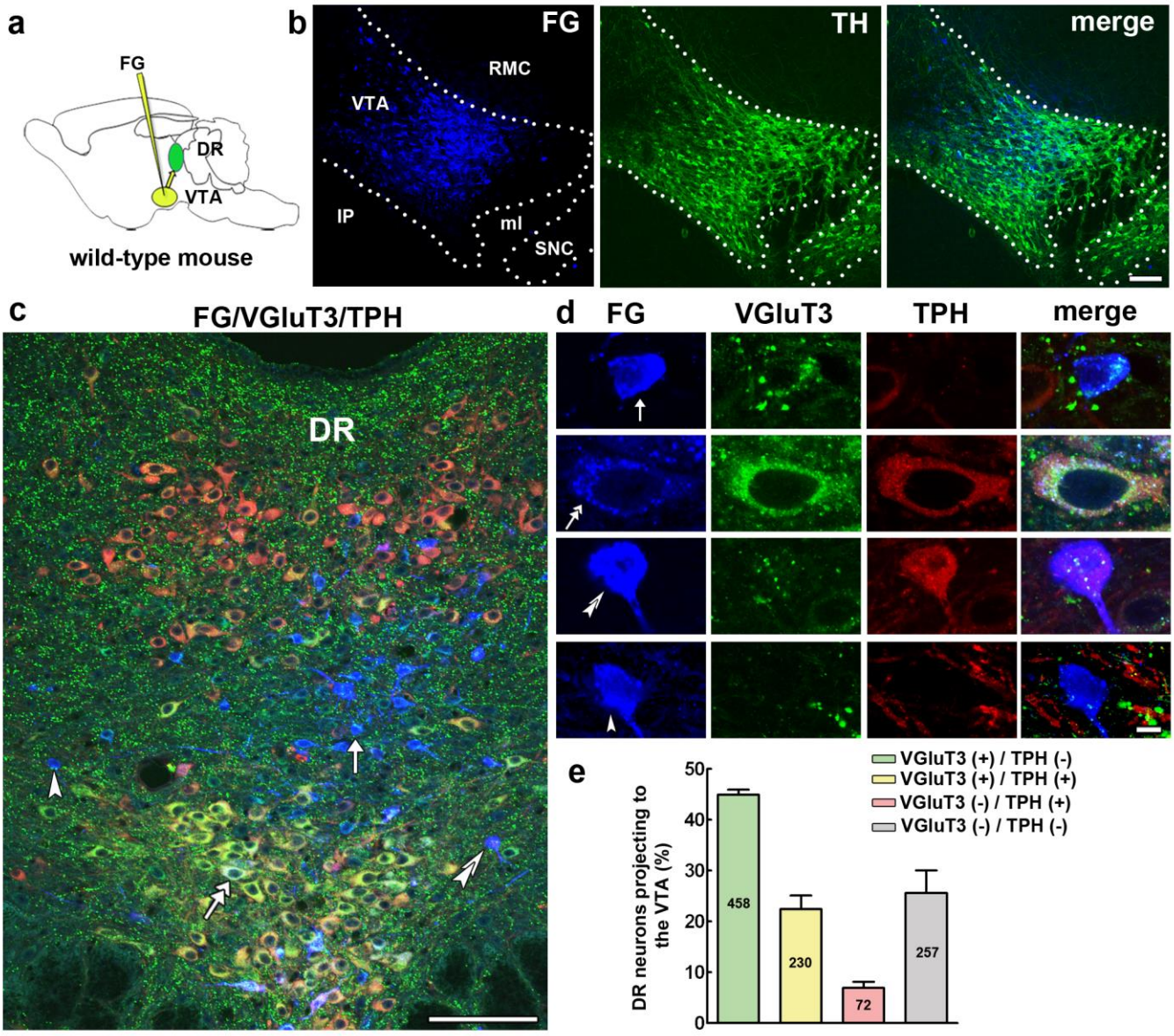

Supplementary Figure 5 Most mouse DR neurons projecting to the VTA express VGluT3.

(a) Retrograde tracer FG was delivered into the VTA (n = 4). (b) FG (blue) injection site within the VTA, which was delineated by tyrosine hydroxylase (TH) immunoreactivity (green). (c) Low magnification of a triple immunolabeled DR coronal section showing FG-IR (blue), VGluT3-IR (green), and TPH-IR (red). (d) Four different phenotypes of labeled neurons are seen at high magnification whose frequency (mean + s.e.m) is shown in e. Among all identified DR neurons projecting to the VTA, 45% expressed only VGluT3, 22% co-expressed VGluT3 and TPH, 7% expressed TPH alone, and 27% lacked both VGluT3 and TPH. FG cell counting was made from between bregma -4.24 and -4.84 mm (8-9 sections per mouse). IP, interpeduncular nucleus; ml, medial lemniscus; RMC, red nucleus; SNC, substantia nigra compact. Diagrams were adapted from mouse brain atlas. Bars: (b and c) 100 μm; (d) 5 μm.

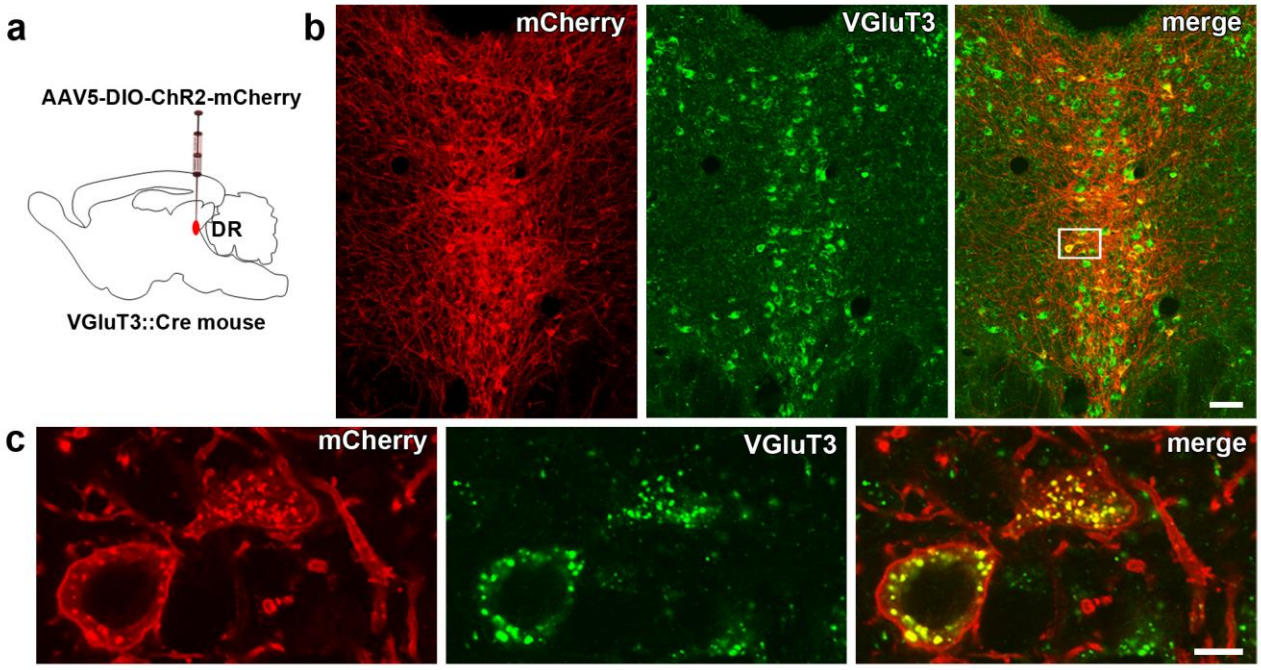

Supplementary Figure 6 DR VGluT3 immunoreactive neurons co-expressed mCherry whose expression was under the regulation of the VGluT3 Promoter (VGluT3-ChR2-mCherry mice).

(a) Schematic representation of AAV5-DIO-ChR2-mCherry injection into the DR of VGluT3::Cre mice. (b) Double labeled DR sections for the detection of mCherry-IR (red) or VGluT3-IR (green). (c) High magnification of area delimited by a white box in b showing cellular detection of mCherry and VGluT3. Bars: (b) 50 µm; (c) 5 µm.

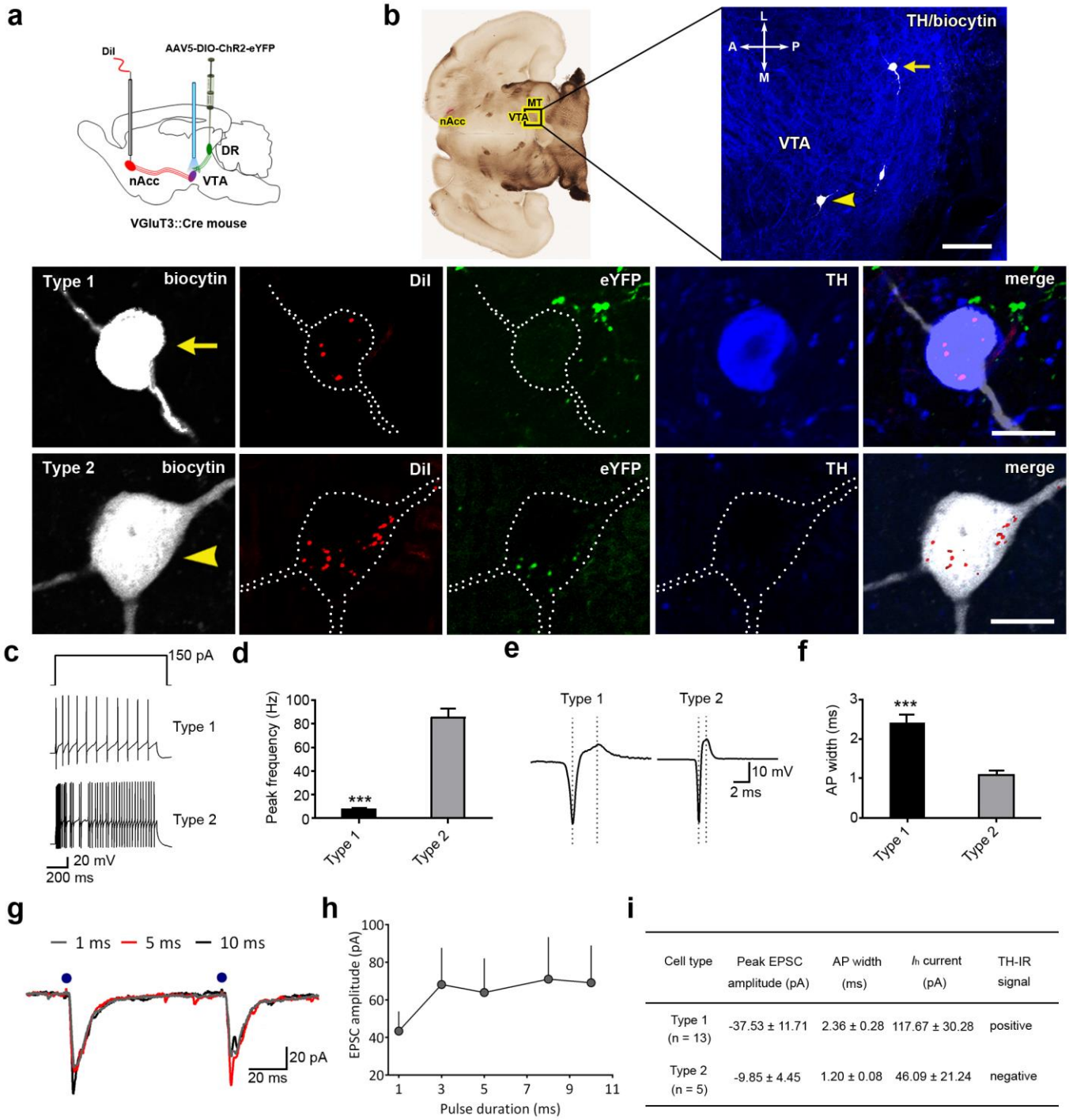

Cell type	Peak EPSC amplitude (pA)	AP width (ms)	I_h current (pA)	TH-IR signal
Type 1 (n = 13)	-37.53 ± 11.71	2.36 ± 0.28	117.67 ± 30.28	positive
Type 2 (n = 5)	-9.85 ± 4.45	1.20 ± 0.08	46.09 ± 21.24	negative

Supplementary Figure 7 Electrophysiological properties of mesoaccumbens neurons innervated by VGluT3 terminals from DR.

(a) DR VGluT3 neurons were infected by injections of AAV5-DIO-ChR2-eYFP into the DR of VGluT3::Cre mice. The retrograde tracer DiI was injected into the nAcc to label individual mesoaccumbens neurons for intracellular recordings. (b) Brain horizontal section, containing biocytin filled cells (white cells) in VTA (TH-IR, blue). High magnification images of the same neurons show DiI labeling (red dots) and the presence (Type 1, arrow), or absence (Type 2, arrowhead) of TH as well as

DR VGluT3 terminals containing eYFP (green). (c) Representative current clamp recordings of action potentials elicited in a Type 1 (TH-positive) and Type 2 (TH-negative) mesoaccumbens neuron during a depolarizing current injection (150 pA, 1 s). (d) Mean peak firing frequency of Type 1 and Type 2 neurons (***P <0.001, unpaired two-tailed t-test). (e) Representative cell attached recordings from a Type 1 and Type 2 neuron. Dashed lines represent the points between which the action potential width was measured. (f) Mean AP widths from Type 1 and Type 2 cells (***P <0.001, unpaired two-tailed t-test). (g and h) Input-output curve of laser pulse duration versus peak EPSC amplitude. (g) Traces from an individual (Type 1 mesoaccumbens neuron) in response to constant laser intensity (set at ~2 mW) and variable pulse duration. (h) Summary input-output curve is shown from a group of Type 1, TH-positive mesoaccumbens neurons (n = 6) indicating that increased EPSC amplitudes were elicited by pulses larger than 3 ms. (i) Properties of recorded DiI-positive neurons with light-evoked EPSCs. Bars: (b) 100 µm; 10 µm for high magnification.

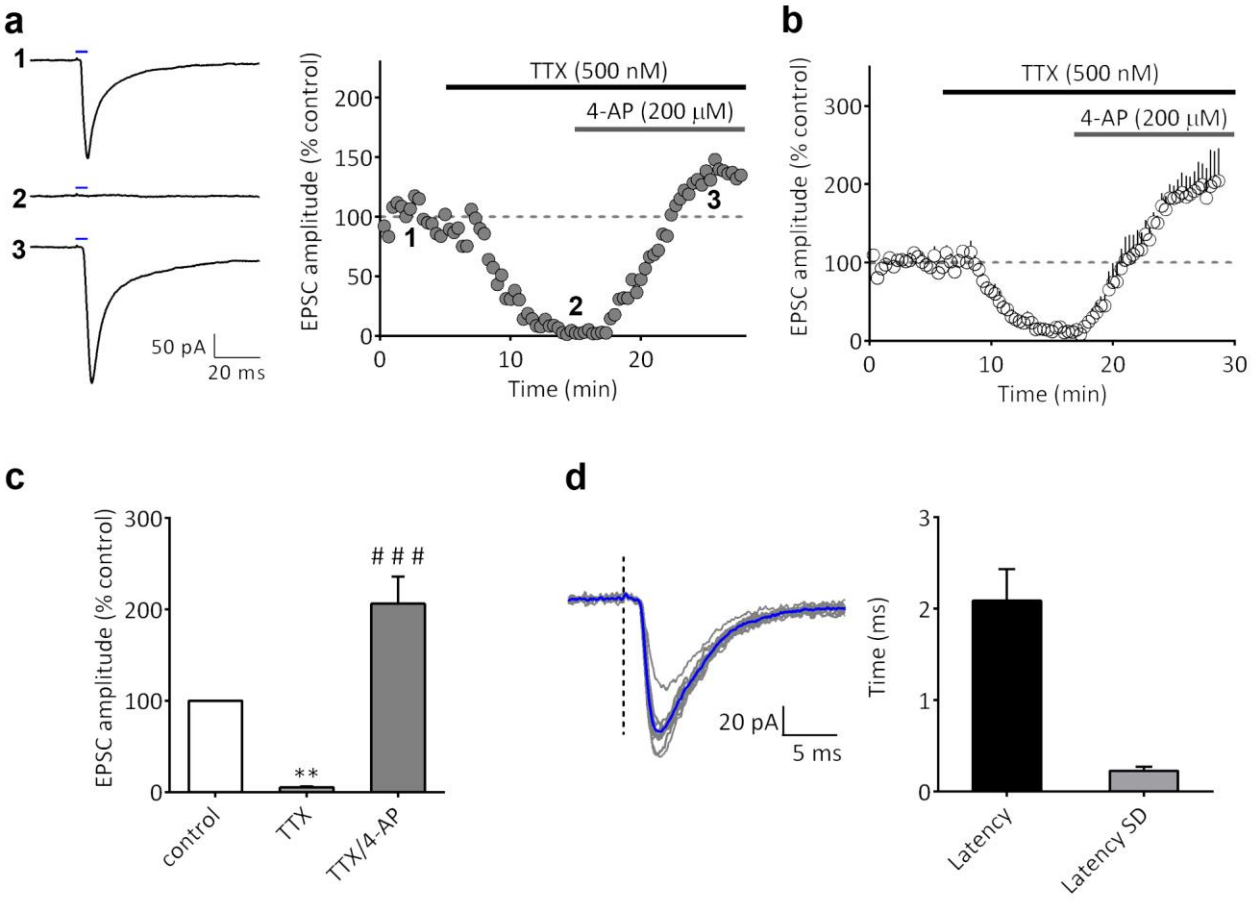

Supplementary Figure 8 Monosynaptic glutamatergic transmission in DR-VTA pathway.

(a) Averaged traces and time course responses of a DiI-positive VTA DA neuron. Optical-evoked EPSCs were eliminated by bath application of TTX (500 nM), and restored by application of 4-AP (200 μM). (b) Summarized time course of the effects of TTX and 4-AP on the optical-evoked EPSCs (n = 7). (c) Summarized bar graph of the effects of TTX (5.4 ± 1.1% to control) and 4-AP (206.4 ± 29.7 % to control) on optical-evoked responses. Repeated measures-ANOVA, $F_{2, 12} = 34.94$, $P < 0.0001$. ** $P < 0.01$ vs control; ### $P < 0.001$ vs TTX, Tukey's *post hoc* comparison. (d) Latency and jitter (standard deviation of latency) of optical-evoked EPSCs. Sample traces of 10 consecutive recordings (gray) and the averaged response (blue) showing low synaptic jitter of the DR-VTA transmissions. Latency was defined as the time from the onset of laser pulses (dashed line) to 10% of the peak responses. Bar graph shows the averaged latency (2.08 ± 0.13 ms, n = 7) and jitter (0.22 ± 0.05 ms, n = 7).

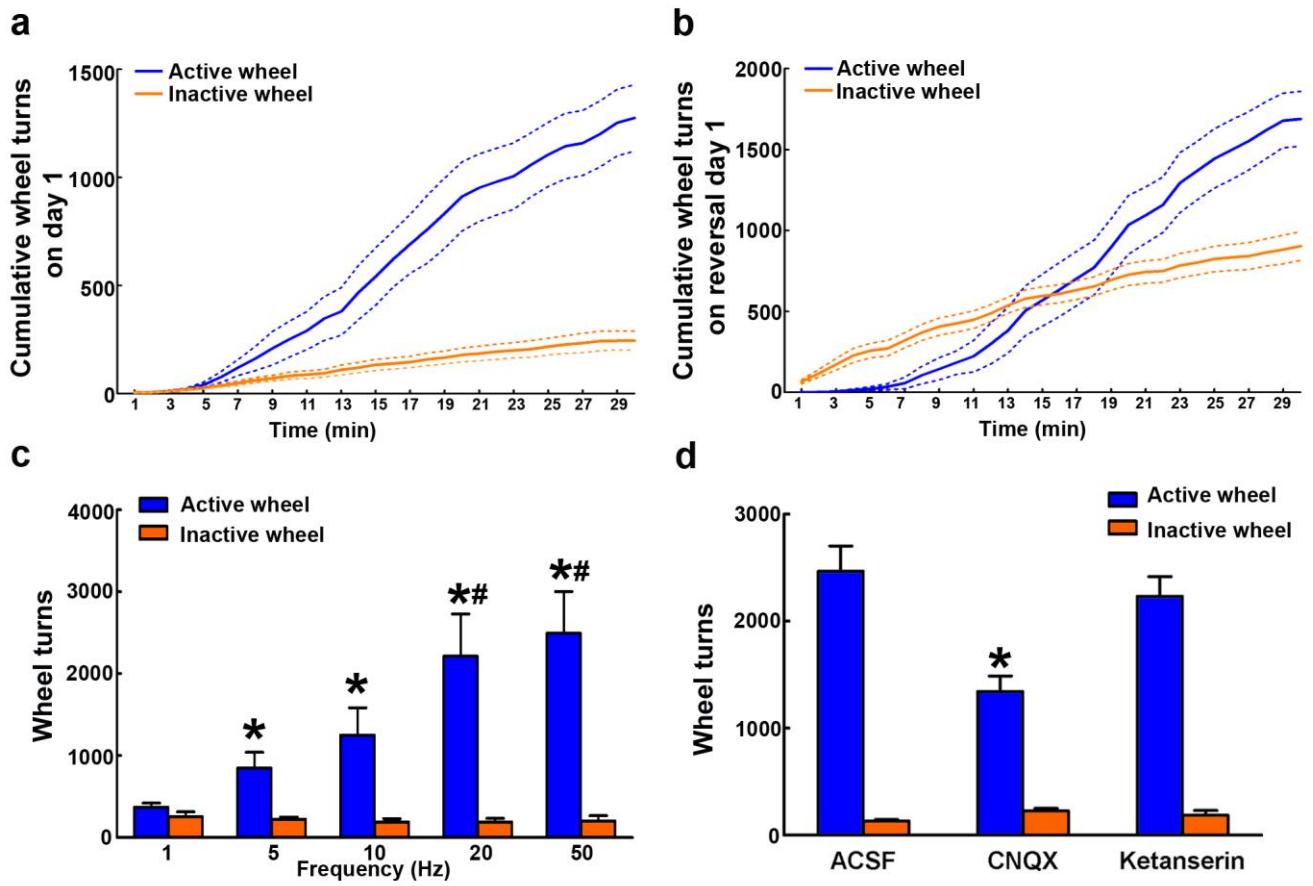

Supplementary Figure 9 Learning and frequency-dependency of the wheel-turning response for VTA light activation of VTA projections from DR VGluT3 neurons.

(a) Cumulative wheel turns on the first day of optical intracranial self-stimulation (oICSS) training. Each turn triggered light stimulation in the VTA of VGluT3-ChR2-eYFP mice (n = 9). Solid lines represent the mean and dashed lines represent ± s.e.m. (b) Cumulative wheel turns made on the first oICSS reversal day (the first reversal session) to obtain light stimulation of DR inputs in the VTA of VGluT3-ChR2-eYFP mice (n = 9). Solid lines represent the mean and dashed lines represent ± s.e.m. (c) Average number of wheel turns at different stimulation frequencies. VGluT3-ChR2-eYFP mice rotated laser active wheel significantly more than inactive wheel at 5 Hz, 10 Hz, 20 Hz, and 50 Hz (n = 8,* $P < 0.05$ versus inactive wheel). Mice made significantly more active wheel turns at 20 Hz and 50 Hz than other frequencies (# $P < 0.05$), however, there is no significant difference between 20 Hz and 50 Hz ($P > 0.05$). Data are presented as mean + s.e.m. and analyzed by two-way ANOVA with Newman-Keuls *post hoc* test. (d) Average number of wheel turns made by trained mice after intra-VTA microinjection of ACSF, CNQX, or Ketanserin (n = 6 each group). CNQX but not Ketanserin inhibited oICSS induced by light activation of VTA VGluT3-inputs (main effect group: $F_{2, 15} = 12.2$, $P < 0.001$, two-way ANOVA; * $P < 0.001$ CNQX vs ACSF; $P = 0.17$ Ketanserin vs ACSF, Newman-Keuls *post hoc* test).

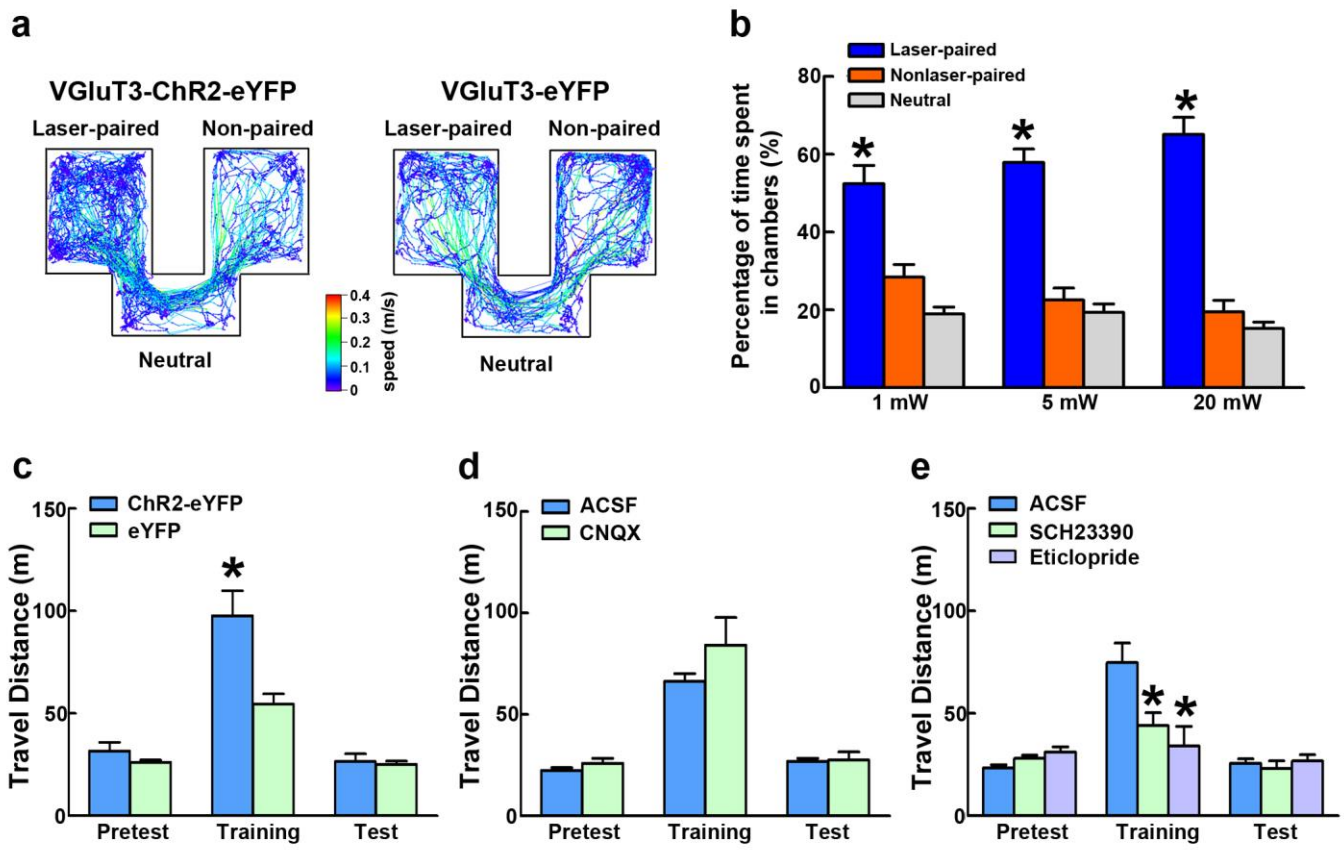

Supplementary Figure 10 Light activation of VTA projections from DR VGluT3 neurons promotes conditioned place preference.

(a) On the test day when laser stimulation was not received, VGluT3-ChR2-eYFP mice returned to and preferred the place where light was given on the previous day. Tracking data show representative traces from a ChR2-eYFP (left panel) or an eYFP (right panel) mouse on test day. (b) VGluT3-ChR2-eYFP mice show significant preference to the laser-associated chamber when stimulated by 1 mW, 5 mW and 20 mW (n = 10, * $P < 0.05$, two-way ANOVA with Newman-Keuls *post hoc* test) at 20 Hz. No significant difference was found between laser stimulation intensities (main effect group: $F_{2,18} = 0$, $P = 1$; main effect chamber: $F_{2,18} = 60.82$, $P = 0.000$; group x chamber interaction: $F_{2,18} = 3.11$, $P = 0.027$, two-way ANOVA). (c) Laser stimulation significantly increased locomotor activity in the VGluT3-ChR2-eYFP mice on laser training day (* $P < 0.05$, two-way ANOVA with Newman-Keuls *post hoc* test). Bars show the average travel distance for each group of mice (ChR2-eYFP mice versus eYFP mice, n = 10 each group). (d) CNQX had no effect on the locomotor activity of VGluT3-ChR2-eYFP mice on laser training day ($P = 0.153$, n = 8 in ACSF group, n = 6 in CNQX group, two-way ANOVA with Newman-Keuls *post hoc* test). (e) SCH23390 and eticlopride each significantly decreased the locomotor activity of VGluT3-ChR2-eYFP mice on laser training day (* $P < 0.05$, n = 7 in SCH23390 group, n = 6 in eticlopride group, n = 7 in ACSF group, two-way ANOVA with Newman-Keuls *post hoc* test). Data are presented as mean + s.e.m.

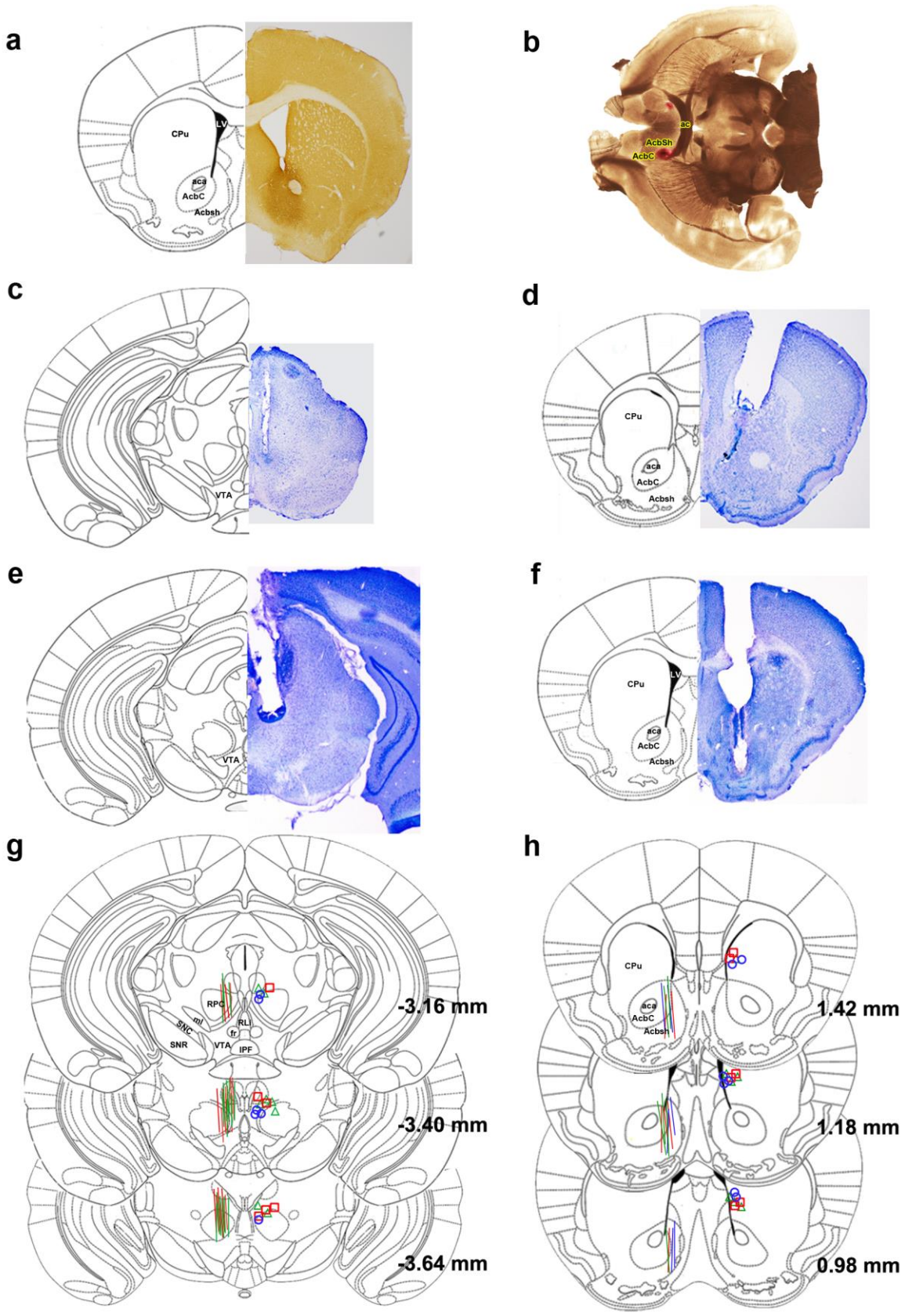
a
CPu
LV
aca
AcbC
Acbsh
b
ac
AcbSh
AcbC
c
VTA
d
CPu
aca
AcbC
Acbsh
e
VTA
f
CPu
LV
aca
AcbC
Acbsh
g
RPC
mt
SNC
SNR
RLi
fr
VTA
IPF
-3.16 mm
-3.40 mm
-3.64 mm
h
CPu
aca
AcbC
Acbsh
1.42 mm
1.18 mm
0.98 mm

Supplementary Figure 11 Localizations of retrograde tract tracer injections, optical fibers, tips of microinjection guide cannula, and microdialysis probes in VGluT3::Cre mouse brain.

(a) Representative coronal section of VGluT3::Cre mouse injected with FG in nAcc. FG was detected by immunohistochemistry (Bregma 1.10 mm). (b) Representative horizontal section of VGluT3::Cre mouse injected with DiI in nAcc. (c) Representative optical fiber track in VGluT3::Cre mouse VTA (Bregma -3.16 mm). (d) Representative microinjection cannula track in nAcc of VGluT3::Cre mouse (Bregma 1.34 mm). (e) Representative microinjection cannula track in VTA of VGluT3::Cre mouse (Bregma -3.40 mm). (f) Representative microdialysis probe track in nAcc of VGluT3::Cre mouse (Bregma 1.10 mm). (g) Optical fibers placements in VTA are indicated by the green (VGluT3-eYFP mice) or red (VGluT3-ChR2-eYFP mice) line segments in the schematic brain drawings. Microinjection cannula tips in VTA are indicated by green triangles (ACSF group), red squares (CNQX group) or blue circles (Ketanserin group) in the schematic brain drawings. fr, fasciculus retroflexus; IPF, interpeduncular fossa; ml, medial lemniscus; RLi, rostral liner raphe; RPC, red nucleus parvicellular part; SNC, substantia nigra compacta; SNR, substantia nigra reticulata part. (h) Microdialysis probes placements in nAcc are indicated by green (ACSF group), red (CNQX group) or blue (AP5 group) line segments in the schematic brain drawings. Microinjection cannula tips in nAcc are indicated by green triangles (ACSF group), red squares (eticlopride group), or blue circles (SCH23390 group) in the schematic brain drawings. aca, anterior commissure anterior part; AcbC, accumbens nucleus core; Acbsh, accumbens nucleus shell; CPu, caudate putamen; LV, lateral ventricle; ml, medial lemniscus. Diagrams were adapted from mouse atlas.

Supplementary Table 1 Percentage of four phenotypes of DR neurons projecting to the VTA

Bregma (in mm)	VGluT3(+)/TPH(-)	VGluT3(+)/TPH(+)	VGluT3(-)/TPH(+)	VGluT3(-)/TPH(-)
-6.84 to -7.08				
Rat # 1	44.76% (*n* = 87)	13.35% (*n* = 24)	11.78% (*n* = 20)	30.10% (*n* = 65)
Rat # 2	45.70% (*n* = 36)	15.77% (*n* = 18)	18.24% (*n* = 16)	29.01% (*n* = 35)
Rat # 3	40.44% (*n* = 76)	15.82% (*n* = 34)	19.92% (*n* = 34)	22.21% (*n* = 29)
Rat # 4	48.72% (*n* = 35)	12.82% (*n* = 7)	14.15% (*n* = 10)	20.51% (*n* = 16)
mean ± s.e.m.	43.19 ± 2.06% (*n* = 234)	14.67 ± 2.24% (*n* = 83)	15.69 ± 2.06% (*n* = 80)	26.45 ± 2.42% (*n* = 145)
-7.20 to -8.16				
Rat # 1	43.20% (*n* = 111)	12.29% (*n* = 33)	10.61% (*n* = 30)	33.90% (*n* = 93)
Rat # 2	41.85% (*n* = 160)	15.68% (*n* = 58)	10.04% (*n* = 39)	32.71% (*n* = 127)
Rat # 3	43.88% (*n* = 327)	14.87% (*n* = 110)	16.67% (*n* = 126)	24.80% (*n* = 188)
Rat # 4	45.36% (*n* = 300)	12.24% (*n* = 82)	13.01% (*n* = 82)	29.39% (*n* = 186)
mean ± s.e.m.	43.70 ± 1.54% (*n* = 898)	13.95 ± 0.83% (*n* = 283)	13.22 ± 1.23% (*n* = 277)	29.26 ± 1.82% (*n* = 594)
-8.28 to -8.40				
Rat # 1	50.86% (*n* = 25)	15.34% (*n* = 8)	8.45% (*n* = 4)	25.34% (*n* = 12)
Rat # 2	49.11% (*n* = 75)	13.62% (*n* = 18)	8.24% (*n* = 12)	30.55% (*n* = 57)
Rat # 3	56.14% (*n* = 39)	16.57% (*n* = 15)	11.20% (*n* = 8)	16.09% (*n* = 9)
Rat # 4	63.19% (*n* = 58)	8.13% (*n* = 8)	8.63% (*n* = 8)	20.04% (*n* = 18)
mean ± s.e.m.	53.14 ± 2.72% (*n* = 197)	13.25 ± 1.98% (*n* = 49)	8.69 ± 0.70% (*n* = 32)	24.92 ± 3.48% (*n* = 96)

Percent refers to the number of FG retrogradely labeled DR neurons expressing VGluT3 mRNA, TPH-IR, co-expressing both VGluT3 mRNA and TPH-IR, or lacking both VGluT3 mRNA and TPH-IR divided by the total number of FG labeled DR neurons. Numbers in parentheses refer to the number of counted neurons in that phenotype condition. FG cell counting was made at three different levels of DR: -6.84 to -7.08 mm from bregma (a total of 12 sections from 4 rats), -7.20 to -8.16 mm from bregma (a total of 26 sections from 4 rats), and -8.28 to -8.40 mm from bregma (a total of 10 sections from 4 rats). *n*, counted neurons.